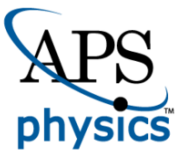

Reduction of Intrinsic Electron Emittance from Photocathodes Using Ordered Crystalline Surfaces

Siddharth Karkare, Jun Feng, Xumin Chen, Weishi Wan, F. Javier Palomares, T.-C. Chiang, and Howard A. Padmore

Phys. Rev. Lett. **118**, 164802 — Published 17 April 2017

DOI: 10.1103/PhysRevLett.118.164802

Reduction of intrinsic electron emittance from photocathodes using ordered crystalline surfaces

Siddharth Karkare, Jun Feng, Xumin Chen, and Weishi Wan
*Lawrence Berkeley National Laboratory, 1 Cyclotron Rd., Berkeley, CA, USA 94720**

F. Javier Palomares
Instituto de Ciencia de Materiales de Madrid (CSIC), Sor Juana Ins de la Cruz, 3, 28049 Madrid, Spain

T.-C. Chiang
Department of Physics, University of Illinois, Urbana, IL 61801 USA and Frederick Seitz Materials Research Laboratory, University of Illinois, Urbana, IL 61801 USA

Howard A. Padmore
Lawrence Berkeley National Laboratory, 1 Cyclotron Rd., Berkeley, CA, USA

The generation of intense electron beams with low emittance is key to both the production of coherent x-rays from free electron lasers, and electron pulses with large transverse coherence length used in ultrafast electron diffraction. These beams are generated today by photoemission from disordered polycrystalline surfaces. We show that the use of single crystal surfaces with appropriate electronic structures allows us to effectively utilize the physics of photoemission to generate highly directed electron emission, thus reducing the emittance of the electron beam being generated.

Laser driven sources of ultrafast pulsed electrons are central to a wide range of instrumentation, such as ultrafast electron diffraction (UED) [1], dynamic transmission electron microscopy (DTEM) [2], x-ray free electron lasers (XFEL) [3] and energy recovery linear accelerator sources of ultra-high brightness x-rays (ERL) [4]. At the heart of these systems is a laser driven photocathode located in a cavity that is designed to produce a high longitudinal electric field. These structures (also known as photoinjectors) are designed to accelerate electrons to a high energy and at the same time preserve the transverse emittance of the electron beam.

Normalized transverse emittance is a key parameter in all these types of sources and is defined as [5], $\epsilon_{nx} = \sigma_x \sigma_{px} / (m_e c)$, where σ_x is the rms laser spot size on the photocathode, σ_{px} is the rms transverse momentum of the emitted electrons, m_e is the rest mass of the electron and c is the speed of light in vacuum. Reduction of the emittance at the cathode is critical to the operation of many electron and x-ray sources. For example, in XFELs the smallest lasing wavelength is limited by the emittance of the electron beam at the cathode[6] and in UED the transverse coherence length which limits the largest lattice size that can be studied is inversely proportional to the transverse emittance[7]. The laser spot size (σ_x) is set either by the ability to focus the drive laser on the cathode or by the electric field at the cathode and the bunch charge required by the application[8] leaving the rms transverse momentum (σ_{px}) as the only parameter that can be changed to minimize emittance.

For polycrystalline cathodes with disordered surfaces, normally used in photoinjectors, the transverse momentum can be calculated within the 3-step photoemission picture[9] as shown by Dowell and Schmerge [10]. This model assumes an isotropic distribution of electron trajectories, a free electron dispersion relation within the material and zero lattice temperature. According to this formulation the rms transverse momentum is given by

$$\sigma_{px} = \left[m_e \left(\frac{\hbar\omega - W}{3} \right) \right]^{\frac{1}{2}}, \tag{1}$$

where $\hbar\omega$ is the photon energy and W is the work function. $\hbar\omega - W$ is defined as the excess energy. For a non-zero temperature T, $\sigma_{px} \to \sqrt{m_e k_B T}$ as the excess energy goes below zero[11]. k_B is the Boltzmann constant. From the same 3-step based photoemission model, it can be shown that the quantum efficiency (QE) is proportional to the square of the excess energy[12]. In the past decade, experimental studies of metal cathodes with normally incident light have validated this model both in terms of QE [12] and emittance [11, 13, 14]. A consequence of this model is that the QE depends on the 4th power of the emittance that is required. Thus, reducing the excess energy to reduce emittance results in a dramatic loss in QE often resulting in impractically high power specifications of the drive laser. The high laser power can also result in increased emittance due to ultrafast laser heating of electrons in the cathode[15].

For decades, techniques like angle resolved photoelectron spectroscopy have utilized the conservation of transverse momentum during photoemission from single crystal ordered surfaces to obtain the electronic structure of such materials and surfaces. However, the use of single crystal ordered surfaces and utilization of the conservation of transverse momentum for achieving directed elec-

tron emission to reduce the rms transverse momentum has largely remained unexplored. Few prior experiments have investigated this direction, however, they have been inconclusive due to insufficient surface preparation[16] or due to a disordered mono-atomic overlayer on the surface[7] or due to inaccurate measurement of the rms transverse momentum[17].

In this letter we show that we can obtain small transverse momentum along with a high QE from single crystal ordered surfaces with a suitable electronic structure by relying on the conservation of transverse momentum during electron emission. We first present a one-step photoemission model that allows us to calculate the QE and the rms transverse momentum from single crystal ordered surfaces. We validate this model against experimental measurements of QE and rms transverse momentum obtained from a Ag(111) surface. Finally we show that the 2-D electron gas formed on an ordered Ag(111) surface can act as an excellent electron source with 2 times smaller rms transverse momentum and nearly the same QE as compared to polycrystalline photocathodes currently used in photoinjectors. The photoemission model presented here can be used in conjunction with electron structure and wave function calculation techniques such as density functional theory to obtain the relevant photoemission properties and to computationally screen single crystal ordered surfaces for use as electron sources in photoinjectors.

We model photoemission as a transition process from an initial independent single electron state to a final time reversed low energy electron diffraction (LEED) state[18, 19] under the perturbation caused by the field of incident light. The rate of the transition is given by the Fermi golden rule as

$$R = \frac{4\pi}{\hbar}\left(\frac{L}{2\pi}\right)^6 \int d^3\vec{k_i} \int d^3\vec{k} M^2 \delta\left(E_f - (E_i + \hbar\omega)\right) F\left(E_i\right) \tag{2}$$

where $\vec{k_i}$ and $\vec{k}$ are the wave vectors of the electron in the initial and emitted state respectively, E_i and E_f are the energies of the initial and final states respectively and $F\left(E_i\right) = \left(1 + \exp\left(\frac{E_i}{k_B T}\right)\right)^{-1}$ is the Fermi-Dirac distribution. We have assumed the Fermi level to be 0. The δ function enforces the conservation of energy. $M = \left|\langle \phi_f \left|\mathcal{H}\right| \phi_i \rangle\right|$ is the overlap integral or the matrix element where ϕ_i and ϕ_f are the wave functions of the initial and final states. The hamiltonian $\mathcal{H}$ is given by

$$\mathcal{H} = -\frac{e\hbar}{m_e c}\left(\vec{A}\cdot\vec{\nabla} + C\vec{A}\cdot\hat{z}\delta\left(z\right)\right) \tag{3}$$

where $\vec{A}$ is the vector potential of light inside the photoemitting surface and C is a constant that takes into account the sudden change in the field of incident light at the surface and depends only on the photon energy and the properties of the solid. The constant C can be obtained using photoemission electron spectroscopy data[20–22]. Since the system exhibits translational invariance in the transverse directions (x and y), $M^2 \propto \delta\left(\left(\vec{k_i} - \vec{k}\right)\cdot\hat{x}\right)\delta\left(\left(\vec{k_i} - \vec{k}\right)\cdot\hat{y}\right)$ enforcing the conservation of transverse momentum.

The QE and rms transverse momentum can be obtained as

$$\mathrm{QE} = \frac{R}{\mathcal{F}L^2} \tag{4}$$

and

$$\sigma_{px} = \left[\frac{\int d^3\vec{k_i}\int d^3\vec{k}\hbar^2 k_x^2 M^2 \delta\left(E_f - (E_i + \hbar\omega)\right) F\left(E_i\right)}{\int d^3\vec{k_i}\int d^3\vec{k} M^2 \delta\left(E_f - (E_i + \hbar\omega)\right) F\left(E_i\right)}\right]^{\frac{1}{2}} \tag{5}$$

where $\mathcal{F}$ is the flux of incident photons per unit area and L is the length of the bounding box used to perform the integrations. Note that QE and rms transverse momentum are independent of L as $L \to \infty$.

The detailed calculations of the matrix elements and hence the QE and rms transverse momentum require the knowledge of the band structure, wave functions and the orientation of the photoemitting surface. These can be obtained for any surface using techniques such as density functional theory or tight binding calculations. This model includes all photoemission effects relating to the polarization of incident light, the angle of incidence and the electronic band structure within the independent electron single body photoemission picture.

We establish the validity of this model by calculating the QE and transverse momentum distributions and comparing them to the experimental values for the Ag(111) surface. When the photon energy is close to the photoemission threshold the conservation of energy and transverse momentum allow only the electrons around the L-point in Ag(111) to be emitted. The band structure of Ag around the L-point in the longitudinal direction can be modeled by a nearly free electron model fit to the upper and lower *sp* bands. In the transverse direction the band structure is assumed to be parabolic and cylindrically symmetric. The wave functions near the L-point can be modeled as plane waves in the transverse directions and as Bloch waves in the longitudinal direction.

The Ag(111) surface exhibits a Shockley surface state within the L-gap due to the abrupt truncation of the lattice at the surface[19]. The wave functions of the surface state can be modeled in a way similar to that of the *sp* band wave functions except the wave vector in the z direction is complex causing the surface state to decay within the bulk of the crystal. The energy of the surface state can change significantly with the sample and surface preparation methods and is sensitive to the strain in the crystal. At room temperature it has been reported to range between -20 meV to -120 meV[23, 24]. Here, we use it as a fitting parameter and obtain the best fit for QE

at surface state energy of −100 meV. The details of the QE and transverse momentum distribution calculations have been presented elsewhere[22].

In order to measure the QE and the transverse momentum distributions, a single crystal Ag(111) sample was prepared in an ultra-high vacuum chamber with base pressure in the low 10^{-10} torr range. Several cycles of Ar ion bombardment (1 keV energy) and annealing to 500°C were performed until a sharp hexagonal LEED pattern was observed. The surface cleanliness was verified using Auger electron spectroscopy. The QE was obtained by measuring the photocurrent and the power of light incident on the sample surface. A laser based plasma lamp with a tunable wavelength monochromator[25] was used as the light source to generate the photoemission in our experiment. The spectral width of the light source was 2 nm FWHM. The transverse momentum distributions were obtained by measuring the spot size of the emitted electron beam after allowing it to drift and expand under the transverse momentum of the emitted electrons post a longitudinal acceleration to several kV. The details of the measurement setup are given elsewhere[26].

Figures 1 a and b show the QE and the rms transverse momentum as a function of the excess energy for the Ag(111) surface. We can see that the calculated QE and rms transverse momentum match the measured values quite well validating our photoemission model. The work function of the Ag(111) surface was chosen to be 4.45 eV in order to obtain the best fit to our data. This value of the work function is in good agreement with previous results [27]. Our photoemission model predicts the detailed features found in the QE and rms transverse momentum spectral response both qualitatively and quantitatively.

Figure 1a shows the QE increases dramatically with the angle of incidence θ_i for p polarized light. This dependence of QE on the angle of incidence in p polarized light in known as the vectorial photoelectric effect[28–31]. Our model explains the origin of this effect quantitatively without the use of any empirical data and attributes it to the variation of the matrix element with the angle of incidence in p polarized light[22]. At angles of incidence close to zero, our model under predicts the QE. This discrepancy could be because of the use of plane waves instead of appropriate block functions to model the transverse part of the wave functions.

Several features present in the QE and rms transverse momentum spectral response shown in figure 1 can be understood in terms of the band structure of Ag(111). Figure 2a shows the band structure of Ag projected along the [111] direction. The pink shaded region is the lower *sp* band filled with electrons. The region shaded in blue is the upper *sp* band which is unoccupied. The solid red line is the surface state (ss). The green curve is the 'free electron parabola' corresponding to a particular photon energy $\hbar\omega$. The bottom of the free electron parabola is located below the vacuum level at an energy of $\hbar\omega$.

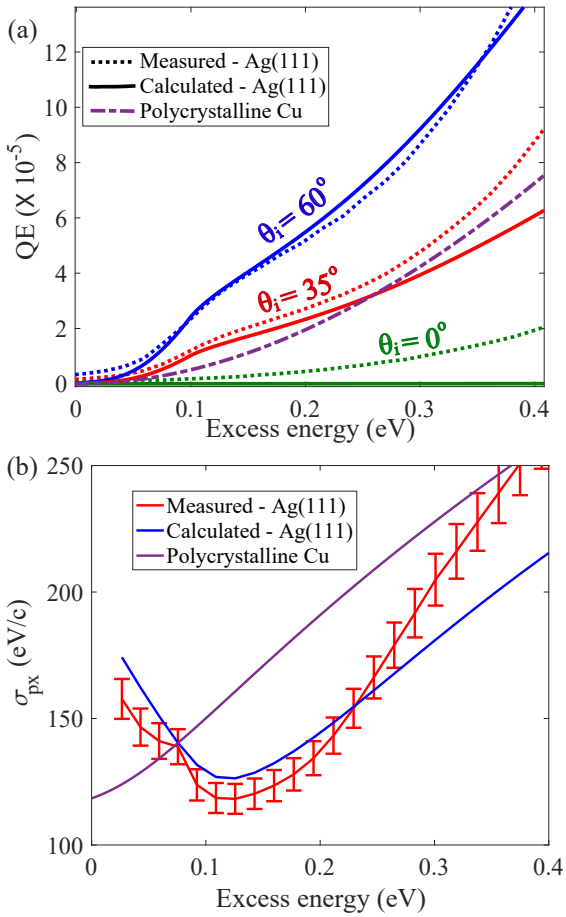

FIG. 1. (a) QE vs excess energy for 3 angles of incidence $\theta_i = 60°$ (blue), $\theta_i = 35°$ (red) and $\theta_i = 0°$ (green). The dotted lines are experimentally measured values and the solid lines are the results from our photoemission model. The experimental measurements have an error bar of 10%. The purple dotted-dashed is the QE measured for a polycrystalline Cu surface[12] (b) rms transverse momentum vs excess energy for the Ag(111) surface. Red curve are the measured values for $\theta_i = 35°$ in unpolarized light. The blue curve is calculated from our photoemission model. The purple curve is the rms tranverse momentum expected from a polycrystalline Cu cathode[11]

For this incident photon energy, the conservation of energy and transverse momentum allow only the occupied states above the corresponding free electron parabola to be emitted.

Figure 2b shows the [111] projected band structure zoomed in near the Fermi level along with 'free electron parabolas' for various excess energies (or incident photon energies). The top most free electron parabola corresponds to excess energy of 0 (or equivalently the incident photon energy equal to the work function W). At this energy we see that no occupied states are present above the free electron parabola. Hence no photoemission is observed at zero excess energy. At an excess energy of ∼35 meV, only the electrons close to the Fermi level in

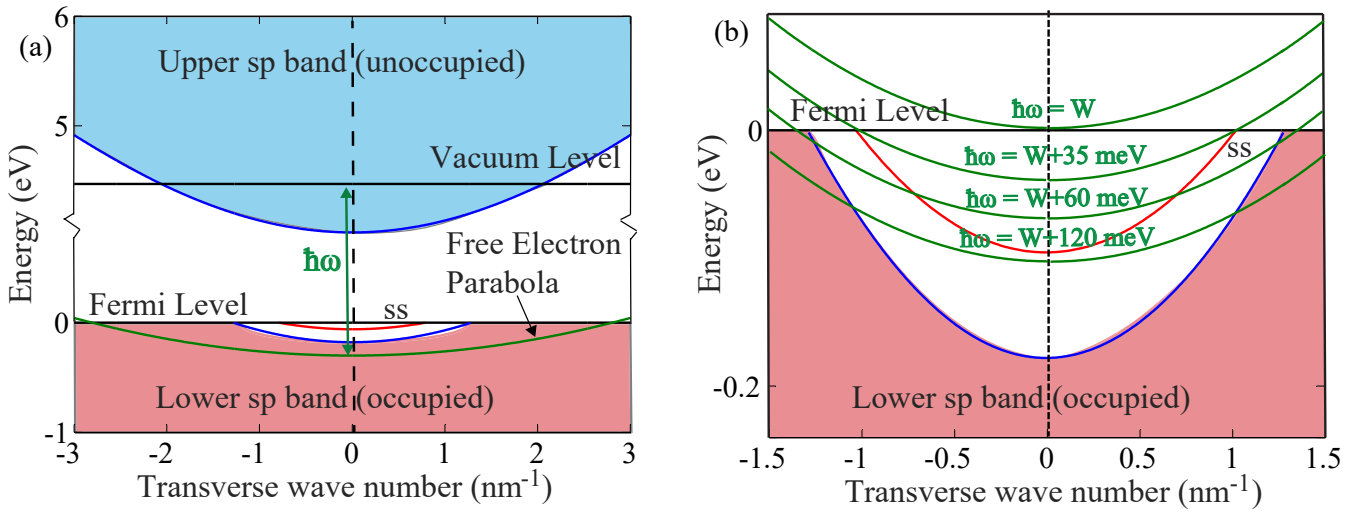

FIG. 2. (a) Band structure of Ag (within the nearly free electron model) projected onto the [111] direction. (b) [111] projected band structure zoomed in near the Fermi level. The 4 green curves are free electron parabolas corresponding to various incident photon energies.

the surface state lie above the free electron parabola and can get emitted. These electrons have a transverse momentum of $\sim$1 nm^{-1}, resulting in a high value of σ_{px}. As the excess energy increases further, more electrons from the surface state with a lower transverse momentum and correspondingly lower energy are allowed to emit, reducing σ_{px} as seen in figure 1b. These surface state electrons are localized at the surface and face minimal scattering before emission. Hence the QE increases rapidly in this region as seen in figure 1a. Beyond an excess energy of 100 meV, electrons from the entire surface state are allowed to emit and the number of electrons emitted from the surface state does not change significantly with excess energy. However, at this point electrons from the bulk states close to the Fermi level are allowed to emit. These bulk electrons have a high transverse momentum causing σ_{px} to increase with increasing photon energy (or excess energy) as seen in 1b. This independence of surface state QE and increase of bulk QE with photon energy results in a knee at $\sim$ 0.1 eV excess energy in the QE spectral response as seen in figure 1a.

The initial decrease in σ_{px} with increasing excess energy is a result of the electronic band structure of the Ag(111) surface. This behavior is remarkably different from the polycrystalline cathode materials where σ_{px} increases monotonically with excess energy. Figure 1 also compares the QE and rms transverse momentum for a polycrystalline Cu cathode, frequently used in photoinjectors, to those obtained from the Ag(111) surface. When operated at an angle of incidence of 60° in p polarized light the Ag(111) cathode gives a QE of $\sim 4 \times 10^{-5}$ at an excess energy of 0.15 eV. For angles of incidence not very close to zero, our photoemission model predicts σ_{px} to be independent of θ_i[22]. Hence from figure 1b we obtain the expected σ_{px} at this excess energy to be 120 eV/c. In order to obtain a similar QE from a polycrystalline Cu cathode, one needs to operate it at an excess energy of 0.3 eV. At this excess energy the expected σ_{px} is nearly 240 eV/c making the emittance from the Ag(111) cathode nearly a factor of 2 better than that obtained from polycrystalline Cu cathodes with the same QE. On the other hand, from figure 1b we see that, to obtain a rms transverse momentum of $\sim$ 120 eV/c from a polycrystalline Cu cathode, it needs to be operated near an excess energy of 25 meV. The QE at this excess energy is in the 10^{-7} range making it impractical for most electron source applications. The value of σ_{px} = 120 eV/c corresponds to an intrinsic emittance of 0.22 μm/mm rms which is very close to the lattice temperature limited value for polycrystalline cathodes[11].

In conclusion we show that it is possible to utilize the conservation of transverse momentum during photoemission from single crystal ordered surfaces to obtain low emittance electron beams. The 2-D electron gas formed on the ordered Ag(111) can act as an excellent electron source providing nearly a factor of two smaller emittance and the same QE as polycrystalline Cu cathodes often used in photoinjectors. Ag(111) surface state emission also turns out to be remarkably robust in ultra-high vacuum conditions with the effects described persisting for weeks, with a simple annealing process for recovering the emission properties. In addition this work points the way to other systems with Dirac cones such as topological insulators and generally systems with reduced electron mass. These systems should have the potential for an order of magnitude reduction in electron emittance.

In practice, using such atomically ordered cathodes should be possible in any photoinjector so long as the

electron gun is equipped with a load-lock along with the ability to switch cathodes and is capable of achieving ultra-high vacuum. Most of the recently developed or planned state-of-the-art DC[32] and RF gun[33, 34] based photoinjectors already have these capabilities. Using atomically ordered surfaces in such photoinjectors should be possible without difficulty.

The photoemission model presented here in conjunction with electronic structure calculation techniques brings forth the possibility of computationally screening for such materials and surfaces that exhibit high QE along with small transverse momentum and hence a reduced emittance. Such a reduction in emittance would have a dramatic effect on applications to x-ray FELs, where the electron energy required for lasing could be substantially reduced, resulting in compact coherent x-ray light sources, or in ultra-fast electron diffraction, where this advantage would be translated into a large transverse coherence length that would enable the observation of ultrafast dynamics in large scale molecular assemblies and proteins.

One of the authors (W. W.) would like to thank Dr. T. Miller for stimulating discussions. This work was supported by the Director, Office of Science, Office of Basic Energy Sciences of the U. S. Department of Energy, under Contract Nos. KC0407-ALSJNT-I0013 and DE-AC02-05CH11231 (W. W., S. K., J. F., H. A. P.) and the U.S. National Science Foundation under Grant No. DMR 13-05583 (T.-C. C.).

* skarkare@lbl.gov

[1] A. H. Zewail, Annu. Rev. Phys. Chem. **57**, 65 (2006).
[2] N. D. Browning *et al.*, ChemPhysChem **11**, 781 (2010).
[3] P. Emma *et al.*, Nat. Photon. **4**, 641 (2010).
[4] D. H. Bilderback *et al.*, New. J. Phys. **12**, 035011 (2010).
[5] M. Reiser, *Theory and Design of Charged Particle Beams* (Wiley-VCH, Weinheim, 2008).
[6] P. Schmser, M. Dohlus, and J. Rossbach, *Ultraviolet and Soft X-Ray Free-Electron Lasers* (Springer, Berlin Heidelberg, 2009).
[7] S. Karkare, L. Boulet, L. Cultrera, B. Dunham, X. Liu, W. Schaff, and I. Bazarov, Phys. Rev. Lett **112**, 097601 (2014).
[8] I. V. Bazarov, B. M. Dunham, and C. K. Sinclair, Phys. Rev. Lett. **102**, 104801 (2009).
[9] C. N. Berglund and W. E. Spicer, Phys. Rev. **136**, A1030 (1964).
[10] D. H. Dowell and J. F. Schmerge, Phys. Rev. ST Accel. Beams **12**, 074201 (2009).
[11] J. Feng, J. Nasiatka, W. Wan, S. Karkare, J. Smedley, and H. Padmore, Appl. Phys. lett **107**, 134101 (2015).
[12] D. H. Dowell, F. K. King, R. E. Kirby, J. F. Schmerge, and J. M. Smedley, Phys. Rev. ST Accel. Beams **9**, 063502 (2006).
[13] Y. Ding, A. Brachmann, F. Decker, D. Dowell, P. Emma, J. Frisch, S. Gilevich, G. Hays, P. Hering, Z. Huang, R. Iverson, *et al.*, Phys. Rev. Lett. **102**, 254801 (2009).
[14] C. P. Hauri, R. Ganter, F. LePimpec, A. Trisorio, C. Ruchert, and H. H. Braun, Phys. Rev. Lett. **104**, 234802 (2010).
[15] J. Maxson, P. Musumeci, L. Cultrera, S. Karkare, and H. Padmore, Nucl. Instrum. Meth. A. **In Press** (2016).
[16] B. L. Rickman, J. A. Berger, A. W. Nicholls, and W. A. Schroeder, Phys. Rev. Lett. **111**, 237401 (2013).
[17] T. C. Droubay, S. A. Chambers, A. G. Joly, W. P. Hess, K. Németh, K. C. Harkay, and L. Spentzouris, Phys. Rev. Lett. **112**, 067601 (2014).
[18] G. D. Mahan, Phys. Rev. B **2**, 4334 (1970).
[19] S. D. Kevan and W. Eberhardt, in *Angle resolved photoemission: theory and current applications*, edited by S. D. Kevan (Elsevier, Amsterdam, 1992).
[20] T. Miller, W. E. McMahon, and T.-C. Chiang, Phys. Rev. Lett. **77**, 1167 (1996).
[21] T. Miller, E. D. Hansen, W. E. McMahon, and T.-C. Chiang, Surf. Sci. **376**, 32 (1997).
[22] S. Karkare, W. Wan, J. Feng, T.-C. Chiang, and H. A. Padmore, Phys. Rev. B **95**, 075439 (2017).
[23] S. D. Kevan and R. H. Gaylord, Phys. Rev. B. **36**, 5809 (1987).
[24] R. Paniag, R. Matzdorf, G. Meister, and A. Goldmann, Surf. Sci. **336**, 113 (1995).
[25] J. Feng, J. Nasiatka, J. Wong, X. Chen, S. Hidalgo, T. Vecchione, H. Zhu, F. J. Palomares, and H. A. Padmore, Rev. Sci. Instrum. **84**, 085114 (2013).
[26] J. Feng, J. Nasiatka, W. Wan, T. Vecchione, and H. A. Padmore, Review of Scientific Instruments **86**, 015103 (2015), http://dx.doi.org/10.1063/1.4904930.
[27] H. Kawano, Prog. Surf. Sci. **83**, 1 (2008).
[28] E. Pedersoli *et al.*, Appl. Phys. Lett. **93**, 183505 (2008).
[29] D. W. Juenker, J. P. Waldron, and R. J. Jaccodine, J. Opt. Soc. Am. **54**, 216 (1964).
[30] G. V. Benemanskaya, M. N. Lapushkin, Y. N. Gnedin, and G. W. Fraser, Il Nuovo Cimento D **16**, 599 (1994).
[31] R. M. Broudy, Phys. Rev. B **3**, 3461 (1971).
[32] C. Gulliford, A. Bartnik, I. Bazarov, L. Cultrera, J. Dobbins, B. Dunham, F. Gonzalez, S. Karkare, H. Lee, H. Li, *et al.*, Phys. Rev. ST. Accel. Beams **16**, 073401 (2013).
[33] F. Sannibale, J. Doyle, J. Feng, D. Filippetto, S. Gierman, G. Harris, M. Johnson, T. Kramasz, D. Leitner, R. Li, *et al.*, Proceedings of IPAC 2016 , TUOCA02 (2016).
[34] E. Pirez, P. Musumeci, J. Maxson, and D. Alesini, Nucl. Instrum. Meth. A. **In Press** (2016).